J. Fluid Mech. (1990), *vol.* 213, *pp.* 95–109
Printed in Great Britain

Single-mode Faraday waves in small cylinders

By DIANE M. HENDERSON AND JOHN W. MILES
Institute of Geophysics and Planetary Physics, University of California, La Jolla, CA 92093, USA

(Received 31 March 1989)

Experiments on single-mode Faraday waves in small rectangular and circular cylinders in which both capillary and viscous effects were significant are reported. Measurements of threshold forcing (for neutral stability) and steady-state wave amplitudes are compared with theoretical predictions. Theoretical predictions of the resonant frequency of a single mode and of the threshold amplitude for its excitation on the hypothesis of linear boundary-layer damping agree well with the measured data. (The theory must use the measured damping rate to predict these quantities for waves in the rectangular cylinder.) Theoretical predictions of wave amplitudes are in reasonable agreement with those observed in the circular cylinder; however, the theory provides only qualitative predictions of amplitudes for waves in the rectangular cylinder. In experiments in which two modes are theoretically admissible, the one with the smaller damping rate is observed; however, a single-mode calculation proves inadequate for the prediction of the stability boundary.

1. Introduction

We consider here those waves (*Faraday waves*) that are subharmonically excited by the vertical oscillation of a cylinder of fluid. Faraday's (1831) original experiments involved multi-mode wavefields, whereas, except as otherwise noted, we consider configurations in which only a single mode is excited. Our objective is to extend previous comparisons between (weakly nonlinear) theoretical predictions and measurements, focusing on (i) the effects of viscosity on neutral stability and dispersion, (ii) the applicability of a theoretical model that includes linear damping (Stokes boundary layers) to waves in small cylinders in which other effects, e.g. capillary hysteresis, may be significant, and (iii) the applicability of single-mode theory in those parametric domains in which either one or two modes are theoretically possible. To this end, we measured wave-damping rates, threshold forcing amplitudes, natural frequencies, and steady-state amplitudes of waves in rectangular and circular cylinders of dimensions such that both viscosity and surface tension were significant. We compare our data with Miles's (1984) theoretical predictions, which we recapitulate in §2.

In earlier experiments, Benjamin & Ursell (1954) and Dodge, Kana & Abramson (1965) found reasonable agreement between their measured threshold amplitudes and the inviscid predictions of Benjamin & Ursell (1954) except for three discrepancies: (i) the inviscid theory predicts a zero threshold amplitude at resonance, whereas the actual waves must surmount a viscous threshold; (ii) the measured bandwidth is narrower than the inviscid prediction; and (iii) the measured resonant frequency is smaller than the inviscid prediction. These discrepancies are typical of viscous effects; however, calculated viscous damping rates were not large

enough to explain them in the earlier experiments. (Benjamin & Ursell 1954 and Dodge *et al.* 1965 did not report measured damping rates.) Dodge *et al.* (1965) also reported amplitude measurements of waves in circular cylinders about twice as large as ours. Virnig, Berman, & Sethna (1988) measured the steady-state amplitudes of waves in large rectangular cylinders in which viscous and capillary effects were small. Their data were in reasonable agreement with the calculations of Gu, Sethna & Narain (1988).

We describe the experimental apparatus and procedures for the present experiments in §3 and our results in §4. First, we show that the measured wave damping is linear and, although larger than, scales like that predicted by a linear boundary-layer analysis. Second, we compare measurements of natural frequencies and threshold (forcing) amplitudes for neutral stability with the viscous predictions. We find that the viscous shift of frequency is as significant as the shift of the threshold amplitude for stability. The calculations fit the data reasonably well for neutral stability of waves in the circular cylinder, but the measured linear damping rate is required for the calculation of neutral stability of waves in the rectangular cylinder. These results support the hypothesis that damping is dominated by linear viscous effects but suggest that linear damping in addition to that due to Stokes boundary layers may be present for waves in the rectangular cylinder. Capillary hysteresis and other nonlinear contact-line effects do not appear to have been significant in our experiments. (See Miles 1967 for a review of wave damping in closed basins.)

Third, we compare the predicted steady-state wave amplitudes with measured data. We find quantitative agreement between theoretical predictions and data for waves in the circular cylinder, but only qualitative agreement for waves in the rectangular cylinder. Finally, we examine a wavefield that comprises only one mode, although two are available (based on the stability calculation) for excitation, and find that the neutral stability calculation does not agree with our experiments; however, the single-mode theory appears to be applicable for calculations of wave amplitudes.

We emphasize that the theory outlined in §2 assumes that both $\epsilon \sim k_1 a_0$ (see (2.4)) and $k_1 a_1$ are small, where a_0 is the amplitude of the prescribed vertical oscillations and a_1 and k_1 are the amplitude and wavenumber of the dominant mode. The forcing parameter in the experiments, $\epsilon \sim 0.05$, was indeed small, but the wave slope $k_1 a_1$ was as large as 0.95/0.75 for the circular/rectangular cylinder. This discrepancy suggests that the weakly nonlinear theory is adequate beyond its putative range of validity for waves in the circular cylinder, but provides perhaps the most likely reason for disagreement between the predicted and measured amplitudes of waves in the rectangular cylinder.

2. Theory

Following Miles (1984) (see also Miles & Henderson 1990 for a review), we expand the surface displacement in the form

$$\eta(\boldsymbol{x}, t) = \sum_{n=1}^{\infty} \eta_n(t)\, \psi_n(\boldsymbol{x}), \tag{2.1}$$

where ψ_n form a complete set of orthogonal modes, normalized according to

$$\iint \psi_m \psi_n \, \mathrm{d}S = \delta_{mn} S, \tag{2.2}$$

S is the cross-sectional area of the cylindrical basin, n is an abbreviation for the pair of numbers that is associated with each mode,

$$\eta_n(t) = \delta_{1n}\, l[p(\tau)\cos\omega t + q(\tau)\sin\omega t] + \frac{l^2}{a_1}[A_n(\tau)\cos 2\omega t + B_n(\tau)\sin 2\omega t + C_n(\tau)] \quad (2.3)$$

is the corresponding generalized coordinate, l is a dimensional lengthscale of order $\epsilon^{\frac{1}{2}}$, where

$$\epsilon = a_0 k_1 \tanh k_1 h \quad (2.4)$$

is a small parameter ($\epsilon \ll 1$ implies weak nonlinearity), a_0 is the dimensional forcing amplitude, h is the water depth, k_1 is the wavenumber of the $n = 1$ mode, and l and a_1 are given by (2.12) and (2.13a). The dominant component of the wavefield is (by definition) the $n = 1$ normal mode with frequency ω and dimensionless amplitudes p and q. Additional modes, with amplitudes of order ϵ, may be present with the forcing frequency 2ω, dimensionless amplitudes A_n and B_n, and mean displacements proportional to C_n. All of the amplitudes depend on the slow time $\tau = \epsilon\omega t$, but $\dot{A}_n$, $\dot{B}_n$, and $\dot{C}_n$ are negligible in the present approximation.

We also introduce the tuning parameter

$$\beta = \frac{\omega^2 - \hat{\omega}_1^2}{2\epsilon\hat{\omega}_1^2} \quad (2.5a)$$

and the bandwidth parameter $\gamma = [1 - (\delta/\epsilon)^2]^{\frac{1}{2}}$, (2.5$b$)

where δ is the ratio of actual to critical damping, and $\hat{\omega}_1$ is the viscous natural frequency (2.18) of the $n = 1$ mode. Neutral stability is determined by $\beta = \pm\gamma$, which implies the threshold forcing amplitude (at which subharmonic waves are excited)

$$a_0 = [k_1 \tanh(k_1 h)]^{-1}\left[\delta^2 + \frac{(\omega^2 - \hat{\omega}_1^2)^2}{(2\omega^2)^2}\right]^{\frac{1}{2}}. \quad (2.6)$$

Steady-state wave amplitudes depend on the relative magnitudes of β and γ. For $0 < \delta/\epsilon < 1$, we have the following configurations:

(i) $\beta > \gamma$: $$p = q = 0, \quad (2.7)$$

(ii) $-\gamma < \beta < \gamma$:

$$p = \pm(\gamma - \beta)^{\frac{1}{2}}\cos(\tfrac{1}{2}\pi + \phi), \quad q = \pm(\gamma - \beta)^{\frac{1}{2}}\sin(\tfrac{1}{2}\pi + \phi), \quad (2.8a, b)$$

$$p = q = 0, \quad (2.8c)$$

(iii) $\beta < -\gamma$: $$p = \pm(-\gamma - \beta)^{\frac{1}{2}}\cos\phi, \quad q = \pm(-\gamma - \beta)^{\frac{1}{2}}\sin\phi, \quad (2.9a, b)$$

$$p = q = 0, \quad (2.9c)$$

where ϕ is determined by $\cos 2\phi = \gamma$.

For (i) the plane surface is stable. For (ii) the wave grows and stabilizes at the steady-state amplitudes given by (2.8a, b). For (iii) the plane surface is stable if the wavemaker starts from rest; however, an initially present wavefield may tend to the amplitudes (2.9a, b).

The dimensional amplitudes a_1, of the ω-component of the wavefield, and a_2, of the secondary, 2ω-component, are related to the dimensionless amplitudes by

$$a_1(\tau) = lN_1[p(\tau)^2 + q(\tau)^2]^{\frac{1}{2}} \quad (2.10)$$

and $$a_2(\tau) = \frac{l^2}{a_1}N_2[A_n(\tau)^2 + B_n(\tau)^2]^{\frac{1}{2}} = \frac{l^2}{a_1}l_2 N_2[p(\tau)^2 + q(\tau)^2]^{\frac{1}{2}}, \quad (2.11)$$

where N_n, the normalization constant implied from (2.2), is $1/J_0(k_{0n}R)$ for axisymmetric waves in the circular cylinder of radius R and $\sqrt{2}$ for one-dimensional waves in the rectangular cylinder,

$$l = 2a_1(\epsilon/|A|)^{\frac{1}{2}}, \tag{2.12}$$

and

$$a_1 = (k_1 \tanh k_1 h)^{-1}, \quad l_2 = \frac{(1+k_1^2 l_*^2)}{\Omega_n(1+k_n^2 l_*^2)}(a_{11n} - \tfrac{1}{4}a_{n11}). \tag{2.13a,b}$$

The coefficient A is given by

$$A = \sum_{n=1}^{\infty}\left[\tfrac{1}{2}a_1 a_{1111} + \frac{(1+l_*^2 k_1^2)}{2(1+l_*^2 k_n^2)}a_{n11}^2 - \frac{4}{\Omega_n}\frac{(1+l_*^2 k_1^2)}{(1+l_*^2 k_n^2)}(a_{11n} - \tfrac{1}{4}a_{n11})^2 + \frac{3}{4}\frac{a_1^2 l_*^2}{(1+l_*^2 k_1^2)}b_{1111}\right], \tag{2.14}$$

where

$$a_{lmn} = C_{lmn}[1 + \tfrac{1}{2}(k_l^2 - k_m^2 - k_n^2)\,a_m a_n], \quad a_{1111} = \tfrac{1}{2}C_{11n}^2 k_n^4 a_1^2 a_n - \tfrac{2}{3}C_{1111}k_1^2 a_1, \tag{2.15a,b}$$

$$C_{lmn} = \frac{1}{S}\iint \psi_l \psi_m \psi_n \,\mathrm{d}S, \quad \Omega_n = 4(\omega/\omega_n)^2 - 1, \quad l_*^2 = (T/g), \tag{2.16a,b,c}$$

$$b_{1111} = \frac{1}{S}\iint (\nabla\psi_1 \cdot \nabla\psi_1)^2 \,\mathrm{d}S, \quad C_{1111} = \frac{1}{S}\iint \psi_1^4 \,\mathrm{d}S, \tag{2.17a,b}$$

and T is the kinematic surface tension. The correlation coefficients C_{lmn} describe the coupling among the normal modes. Table 1 lists the required coefficients for the present experiments. For waves in the rectangular cylinder, the only non-zero correlation coefficient occurs for interactions of the dominant mode with its superharmonic. The dominant axisymmetric mode in the circular cylinder may interact significantly with its first few harmonics.

The above calculations incorporate linear damping on the assumption that viscous effects are confined to thin, laminar boundary layers at the free surface and along the wetted surface of the fluid cylinder. The dominant effects of linear damping are an exponential decay in wave amplitude at a rate γ_0 and a dependence of the dispersion relation on γ_0. For capillary–gravity waves, the viscous dispersion relation is

$$\hat{\omega}_{lm} = \omega_{lm}(1-\delta) = (1-\delta)\,[(gk_{lm} + Tk_{lm}^3)\tanh k_{lm} h]^{\frac{1}{2}}, \tag{2.18}$$

where ω_{lm} is the inviscid natural frequency of the (l, m) normal mode, k_{lm} is the corresponding wavenumber, $\hat{\omega}_{lm}$ is the viscous-shifted frequency, and $\delta = \gamma_0/\omega$. In the rectangular cylinder the wavenumber of the (l, m) mode is $k_{lm} \equiv [(l\pi/a)^2 + (m\pi/b)^2]^{\frac{1}{2}}$, and the cross-sectional area is $S = ab$. For the circular cylinder, l and m indicate the number of nodal diameters and nodal circles, respectively, and k_{lm} is the mth positive zero of $J_l'(k_{lm}R)$ (where J_l' is the derivative of the lth-order Bessel function).

Analytical estimates of δ are available (Miles 1967). In the present model, the boundary layer at the surface corresponds to a surface film that is free to move vertically but cannot stretch horizontally, which implies

$$\gamma_0 = \left(\frac{\nu\omega_{lm}}{2}\right)^{\frac{1}{2}}\left[\frac{k_{lm}}{\sinh 2k_{lm}h} + \frac{k_{lm}\cosh^2 k_{lm}h}{\sinh 2k_{lm}h} + \alpha_s\right]. \tag{2.19}$$

Correlation Coefficient	Rectangular cylinder	Circular cylinder
C_{111}	0	−0.8746
$C_{112} = C_{211}$	0.707	+0.8868
$C_{113} = C_{311}$	0	−0.0106
$C_{114} = C_{411}$	0	−0.0011
C_{1111}	1.500	+2.5515
b_{1111}	1.500 k_1^4	−0.6249 k_1^4

TABLE 1. Correlation coefficients for spatial mode coupling in rectangular and circular cylinders.

The first, second and third terms in the square brackets represent damping in the bottom, free-surface and sidewall boundary layers. It is the sidewall boundary layers that cause γ_0 to depend on the modal structure of the wavefield. For example,

$$\alpha_s = \frac{1}{2R}\left[\frac{1+(l/k_{lm}R)^2}{1-(l/k_{lm}R)^2} - \frac{2k_{lm}h}{\sinh 2k_{lm}h}\right] \tag{2.20}$$

for waves in a circular cylinder, while

$$\alpha_s = \frac{1}{2a}\left(\frac{\omega_{l0}}{\omega_{lm}}\right)^{\frac{1}{2}} + \frac{1}{2b}\left(\frac{\omega_{0m}}{\omega_{lm}}\right)^{\frac{1}{2}} \tag{2.21}$$

for a rectangular cylinder.

3. Experimental apparatus

The apparatus comprised glass rectangular and circular cylinders, an electromagnetic shaker with feedback, and wave gauges. The circular cylinder had a radius of $R = 3.725$ cm. The rectangular cylinder was 8.870×3.205 cm^2, joined by silicone at the corners, where a meniscus was visible. The fluid depth varied between 1.000 cm and 2.050 cm. (These lengths are accurate to ± 0.002 cm.)

The fluid was distilled water, filtered of organics and particles greater than 0.2 μm, with Kodak Photo Flo 200 solution added in the ratio of 80:1 (water:Photo Flo). Photo Flo allowed the fluid to slide along the glass walls with a constant orientation; without it, the water sometimes (irreproducibly) pinned at the glass walls, perhaps because of microscopic defects in the glass. Photo Flo also produced a film at the surface, which we inferred from the fact that bubbles arriving at the surface required about one minute to pop. This delay compares with minimum delays of 0.5 s for a contaminated surface and 0.01 s for a clean surface, reported by Scott (1979) and Kitchener & Cooper (1959), respectively, which suggests (and we believe) that our films were saturated (inextensible). The static surface tension at the fluid–air interface, measured with a Fisher, Model 20 tensiometer, was 42.3 dyn/cm (at 23 °C). The viscosity of the fluid, although unknown, presumably approximated that of pure water, $\nu = 0.01$ cm^2/s. We use this value in (2.19) to calculate linear damping rates for subsequent comparisons with theory unless otherwise stated. We sometimes found it necessary to use measured damping rates, in which cases we used (2.19) to calculate an effective viscosity. We measured the damping rates by stopping the wavemaker, recording the temporal decay of the wavefield, and complex-demodulating the time series to obtain the instantaneous wave amplitudes for the ω-component. (See Bloomfield 1976, pp. 118–150 for a discussion of complex

demodulation.) The mechanical properties of the wavemaker limited our measurements of damping rates to waves with frequencies less than about 10 Hz.

The wavemaker, which drove the cylinder vertically, was an electrodynamic shaker, Bruel & Kjaer Mini Shaker Type 4810. Its horizontal accelerations were not measured; however, according to specifications, transverse accelerations are less than 3% of axial accelerations for frequencies up to 5 kHz. A non-contacting proximity sensor (Kaman model KD-2310) monitored the shaker motion and provided a signal to a servo-controller. The controller acted as a feedback device to ensure that the actual motion followed the programmed one; additionally, it provided measurements of the forcing amplitude, accurate to 0.005 mm. A Digital Equipment Corporation VAXstation II computer system provided the command signal to the shaker. The computer had analog input and output devices, as well as two real-time clocks for separate sampling and command frequencies.

An *in situ*, capacitance-type gauge measured a time series of the surface displacement. It had a diameter of 1.15 mm (the smallest wavelength measured is about 10 mm) and is accurate to 0.01 mm. We filtered the gauge signal through two channels of a Krohn-Hite Model 3323 low-pass, analog filter, which also produced a 20 db gain, and digitized it with the computer. We then subtracted the cylinder motion at frequency 2ω from the filtered signal, since the gauge was not attached to the cylinder. To examine the amplitude evolution of the different components of the wavefield, we complex-demodulated the time series at the forcing frequency 2ω and the wavefield frequency ω. We calibrated the gauge by comparing the distance from the quiescent fluid surface to the wave crest, measured with a mechanical point gauge, to the corresponding voltage response from the capacitance gauge. The mechanical point gauge is a Lory Type C combined with a dial-micrometer accurate to 0.01 mm. The point gauge also monitored the water depth.

4. Results

We now compare theory and experiment for linear damping rates, threshold (forcing) amplitudes and steady-state wave amplitudes.

4.1. *Viscous damping rates*

Figure 1 shows the results of a damping experiment, for a 7 Hz wave in the circular cylinder. Figure 1 (*a*) is the time series; figure 1 (*b*) is the amplitude of the envelope. The slope of the decaying amplitude curve in figure 1 (*b*) is the linear damping rate, γ_0, which is constant within $\pm 8\%$ for each experiment. Although the decay appears to be linear, the rate is 1.65 times larger than predicted by (2.19) with $\nu = 0.01$ cm^2/s. Figure 2 (*a*) shows measured and calculated damping rates as a function of wave frequency for additional experiments in the circular cylinder. The bandedness of the calculated values is a consequence of (2.20), which predicts that radial nodes increase the damping rate. The measured values verify this prediction for the first two, well-separated modes, (0, 1) and (3, 0). The next two modes, (1, 1) and (4, 0), have nearly the same wavenumber; nevertheless, only the (1, 1) mode, which has the lower calculated damping rate, was excited in the experiments. Similarly, when the (5, 0) and (2, 1) modes were both available, the mode with the lower calculated damping rate, (2, 1), was observed. (The modal structure was not resolvable for wavefields with frequencies above 8 Hz). These experiments imply that when two modes are closely spaced but have different damping rates due to the sidewall boundary conditions, the mode with the smaller γ_0 will be excited. In addition, (2.19) and (2.20)

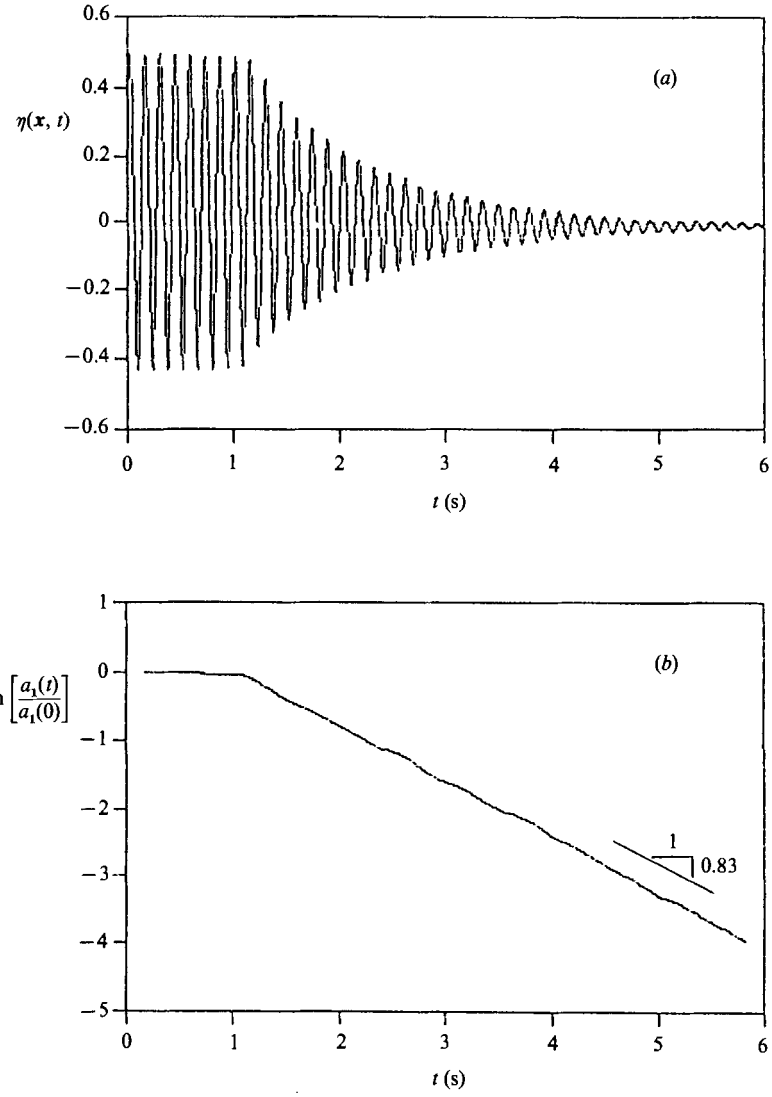

FIGURE 1. Measurements of wave damping when the wavemaker is stopped abruptly (circular cylinder with $\omega/2\pi = 7.00$ Hz and $h = 2.04$ cm). (*a*) Surface displacement. (*b*) Natural logarithm of the complex-demodulated amplitudes a_1, normalized by the steady-state amplitude $a_1(0)$; $\gamma_0 = 0.83\ \mathrm{s}^{-1}$.

adequately predict γ_0 if ν is replaced by an effective value of 0.03 cm^2/s. We remark that (2.19) neglects the variations in surface tension that result from the straining of the surface film. Miles (1967) reports that these surface-tension gradients increase the damping rate by as much as a factor of two, and in the experiments in the circular cylinder the measured damping rates are about 1.7 times larger than that predicted by (2.17).

Figure 2(*b*) shows similar results for wave damping in the rectangular cylinder but with three differences. First, the modal dependence of γ_0 is not as pronounced, and it produces a raggedness, rather than a bandedness, in the calculations. Second, the measured damping rates are much larger, and the effective coefficient of viscosity is an order of magnitude higher than that of water. Third, although the damping is

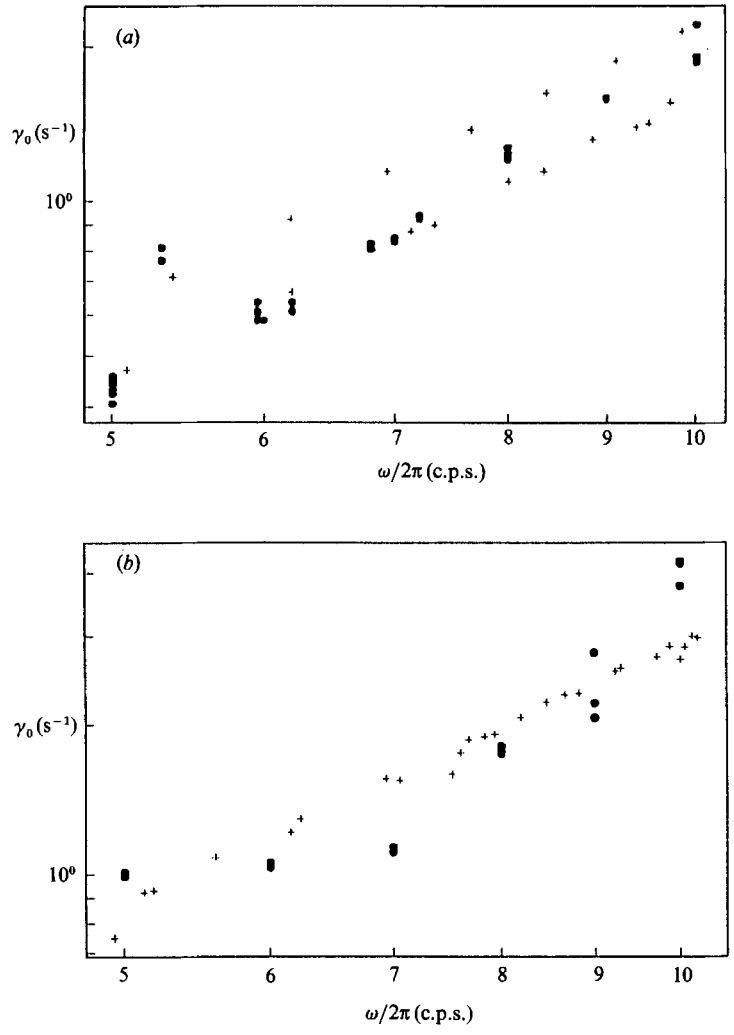

FIGURE 2. Linear damping rates γ_0 as a function of wave frequency $\omega/2\pi$ with $h = 2.04$ cm. ●, data. (*a*) Circular cylinder; +, calculations for normal modes with $\nu = 0.03$ cm^2/s. (*b*) Rectangular cylinder; +, calculations for normal modes with $\nu = 0.1$ cm^2/s.

linear, the dependence of γ_0 on frequency is not predicted adequately by (2.19). The waves in the rectangular cylinder seem to be affected by additional (to that from laminar boundary layers) damping.

4.2. *Neutral stability*

Figure 3 shows the neutral stability curves as a function of forcing amplitude a_0 and wavefield frequency $\omega/2\pi$ for the $(0, 1)$ modes in the circular (figure 3*a*) and rectangular (figure 3*b*) cylinders. These stability boundaries predict a_0 for a given forcing frequency 2ω at which the (l, m) mode with frequency ω will be excited. In these experiments, the wavenumber, wave frequency and forcing amplitude were known; the natural frequency $\hat{\omega}_{01}$ was calculated from (2.18), and δ was both calculated from (2.19) and measured as described in §3. The differences between the viscous and inviscid curves in figure 3 show that viscosity shifts the inviscid

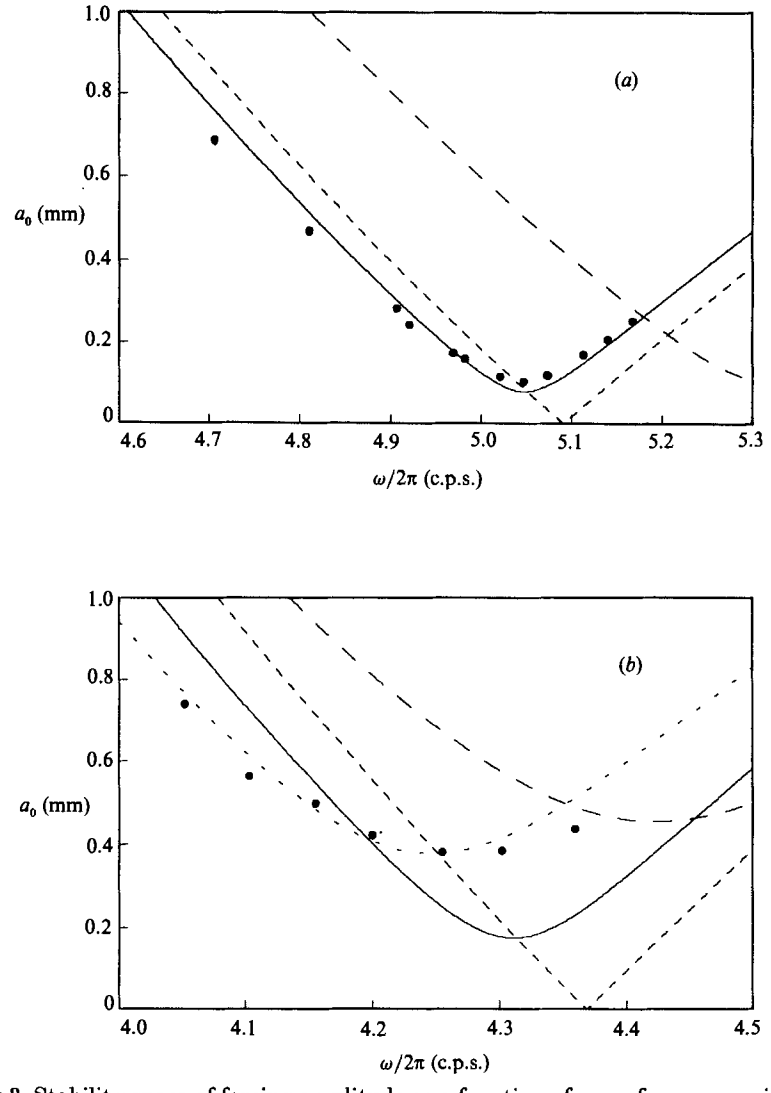

FIGURE 3. Stability space of forcing amplitude as a function of wave frequency with measured (●) and calculated stability boundaries. (*a*) Circular cylinder with $h = 2.04$ cm: ——, calculations with $k_{01} = 1.03$ cm^{-1} and $\delta = 0.008$; – – –, $k_{01} = 1.03$ cm^{-1} and $\delta = 0$; ———, $k_{30} = 1.13$ cm^{-1} and $\delta = 0.012$. (*b*) Rectangular cylinder with $h = 1.0$ cm: - - -, $k_{01} = 0.98$ cm^{-1} and $\delta = 0.028$ (measured damping ratio); —, $k_{01} = 0.98$ cm^{-1} and $\delta = 0.013$ (calculated damping ratio); – – –, $k_{01} = 0.98$ cm^{-1} and $\delta = 0$; ———, $k_{11} = 1.04$ cm^{-1} and $\delta = 0.037$ (measured damping ratio).

prediction of resonant frequency (the resonant frequency corresponds to the minimum of the curve), raises the minimum threshold amplitude to a positive value, and decreases the bandwidth for waves.

A comparison between the solid curves and the data in figure 3(*a*) shows that (2.6) and (2.19) predict the measured stability fairly well for the (0, 1) mode waves in the circular cylinder. For this case, the predicted and measured natural frequencies are indistinguishable. We note that for these waves, the measured damping rate is about 1.65 times larger than predicted by (2.19); however, calculations from (2.6) with the measured damping rate predict a natural frequency that is about 0.4% less than

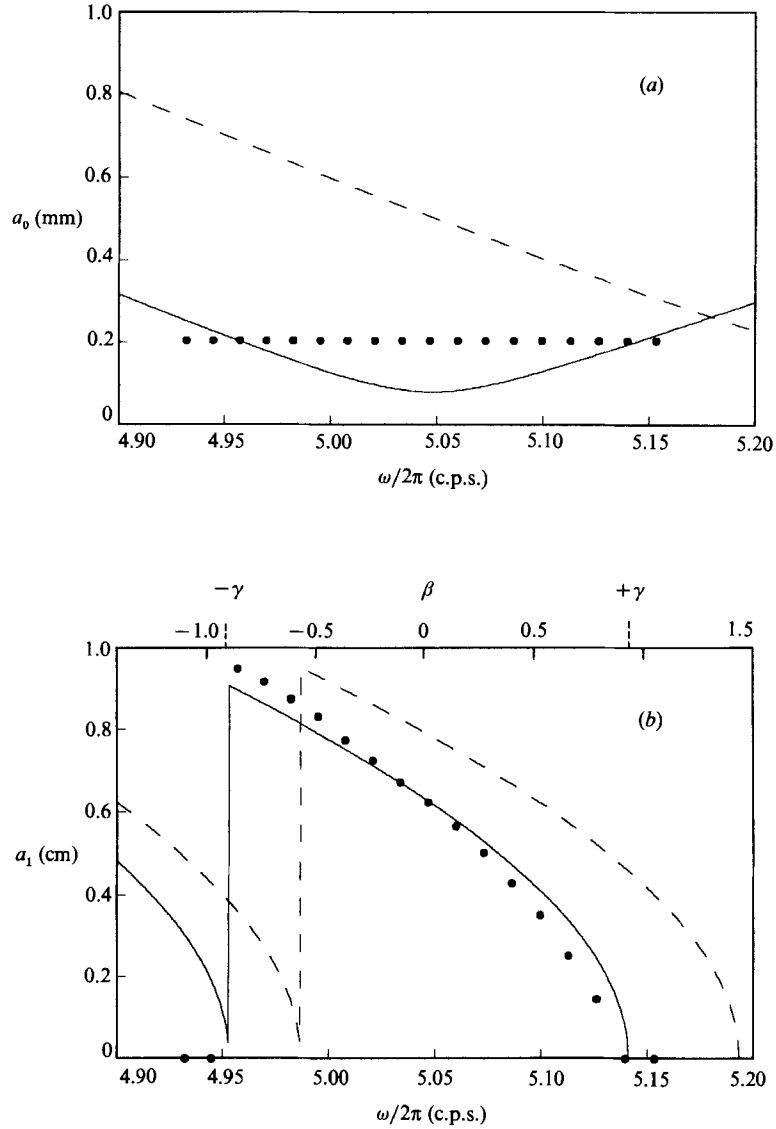

FIGURE 4. Experiments on the (0, 1) mode in the circular cylinder with $h = 2.04$ cm. (*a*) Stability boundaries: —, $k_{01} = 1.03$ cm^{-1} and $\delta = 0.008$; ———, $k_{30} = 1.13$ cm^{-1} and $\delta = 0.012$; ●, locations of the experiments with $a_0 = 0.203$ mm. (*b*) Steady-state wave amplitudes: —, calculations with $\delta = 0.008$; – – –, calculations with $\delta = 0$; ●, measurements.

observed. In contrast, for the (0, 1) mode in the rectangular cylinder (figure 3*b*), (2.6) adequately predicts the measured stability only if the measured linear damping rate is used. (The measured damping rate was about twice as large as predicted by (2.19) and corresponds to an effective viscosity of $\nu = 0.045$ cm^2/s.) For waves in the rectangular cylinder the predicted natural frequency is within 0.7% of that observed. The measured bandwidth is wider than predicted; for $\omega > \hat{\omega}_{lm}$ the calculations overpredict the threshold amplitude. In both cylinders, those waves in experiments for which $\omega < \hat{\omega}_{lm}$ were more likely to become unstable, even near the threshold forcing amplitude. In particular, the waves corresponding to the first two

points in figure 3(*a*) broke after excitation. The high-frequency limit on the data is in accord with predictions; forcing at frequencies above this limit excited the next normal mode.

Our results imply that a linear damping model is adequate for the prediction of the neutral stability of Faraday waves in small cylinders. The Stokes boundary-layer analysis was adequate for waves in the circular cylinder, while the measured damping rate was required for waves in the rectangular cylinder. For experiments in larger cylinders, viscous considerations are less important. However, Virnig *et al.* (1988), whose experiments were conducted in a much larger rectangular tank, report that the addition of Photo Flo to their water caused a slight decrease in both frequency and wave amplitudes. They had incorporated the new surface tension in their calculations, but not a different viscosity. It is possible that additional viscous damping caused the observed decreases; however, calculations from (2.19) and (2.21) would require an effective coefficient of almost $\nu = 1$ cm^2/s (an order of magnitude larger than observed herein, and two orders of magnitude larger than that of water). If viscosity was responsible, this large coefficient, reminiscent of an eddy viscosity, suggests that the boundary layers in their experiments (and perhaps in the present experiments) were turbulent, rather than laminar. (For the experiments of Virnig *et al.*, the wave Reynolds number $Re = \omega/\nu k^2$, is of order 10^4. For the present experiments, $Re \sim 10^3$.)

4.3. *Wave amplitudes*

Figure 4(*a*) shows the location in stability space of experiments on the (0, 1) mode in the circular cylinder with $a_0 = 0.0203$ cm. Measurements of the steady-state wave amplitudes a_1 for these experiments are shown in figure 4(*b*) as a function of both wave frequency and the tuning parameter β. The addition of the viscous damping rate from (2.19) allows (2.8) and (2.10) to adequately predict the wave amplitudes for $-\gamma < \beta < +\gamma$. No wavefields were excited for $\beta < -\gamma$ or $\beta > +\gamma$, as predicted by (2.7) and (2.9*c*). We note that, although the theory assumes weak nonlinearity in wave slope as well as in ϵ, (2.4), predictions are in reasonable agreement with the data for wave slopes as large as 0.95. (The calculations in figure 4(*b*) use the predicted damping rate (2.19); calculations that use the measured damping rate predict amplitudes that are about 0.8 times as large as those observed.)

Predictions of amplitudes for waves in the rectangular cylinder do not agree as well with the measurements as those for the circular cylinder. In figures 6–9 we use the predicted damping rate (2.19) in the calculations and note that the measured damping rates result in predictions of wave amplitudes that are about 0.5 times as large as those observed. Figure 5 shows the location in stability space of four (three are distinguishable) sets of experiments with different forcing amplitudes. The lower limit on the frequency band in each set of experiments corresponds to the frequency below which the wavefield became unstable. That is, the wavefield evolved from the (0, 1) mode to some nonlinear mode that had a hump of fluid at the $x = 0$ end of the tank and sloshed back and forth with one node in the y-direction; accordingly, an amplitude measurement was not significant. The upper limit corresponds to the frequency above which the (1, 1) mode was excited.

Figure 6 shows amplitudes a_1 for waves in set II of figure 5 as a function of wave frequency and the tuning parameter. As in the circular cylinder, the wave amplitudes decrease with increasing frequency, in qualitative accord with the theoretical predictions; however, the decrease in amplitude with frequency is steeper than predicted. Figure 5 shows that these experiments are located in stability space near the intersection of the neutral stability curves for the (0, 1) and (1, 1) modes. Ciliberto

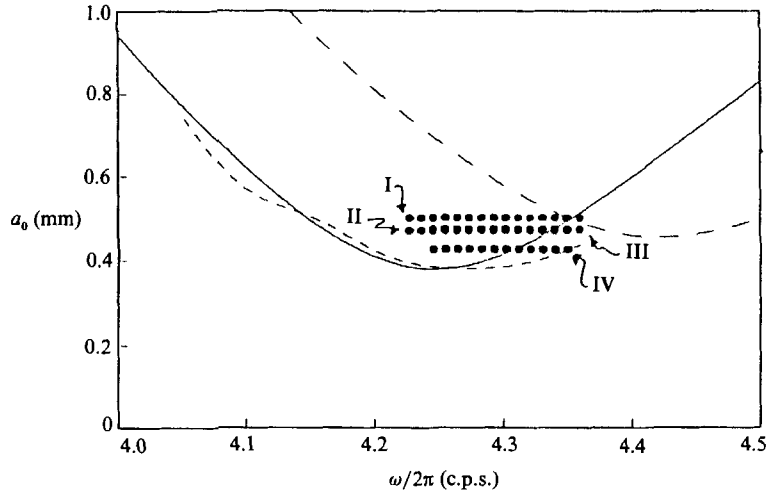

FIGURE 5. Stability space for four sets (I–IV) of experiments on the (0, 1) mode in the rectangular cylinder with $h = 1.0$ cm. Stability boundaries: —, $k_{01} = 0.98$ cm^{-1} and $\delta = 0.028$ (measured damping ratio); ———, $k_{11} = 1.04$ cm^{-1} and $\delta = 0.037$ (measured damping ratio); – – –, measured boundary (cubic-spline fit through data in figure 3*b*); ●, locations of experiments with $a_0 = 0.500$ mm (I), 0.473 mm (II), 0.470 mm (III), and 0.425 mm (IV).

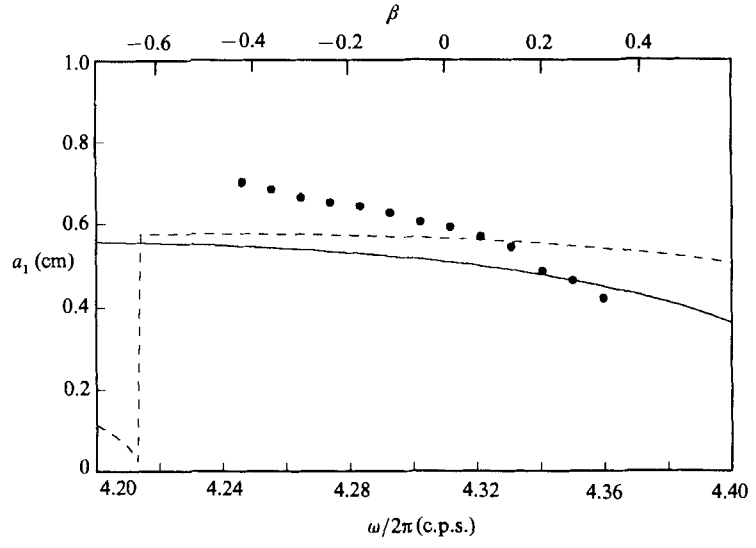

FIGURE 6. Experiments II: wave amplitudes for the (0, 1) mode in the rectangular cylinder with $a_0 = 0.473$ mm; ●, data; —, calculations with $\delta = 0.013$; – – –, calculations with $\delta = 0$.

& Gollub (1985), who observed the interaction between the (4, 3) and (7, 2) modes in a circular cylinder, report that wavefields located near the intersection of two stability boundaries may become chaotic, which suggests that the single-mode theory is inapplicable in this domain.

The amplitudes of waves from sets III and IV indicated in figure 5 are presented in figure 7, which also shows the viscous prediction of wave amplitudes as a function of wave frequency. These results are essentially the same as those for waves in set II, except that the decrease in wave amplitudes with increasing frequency is less steep

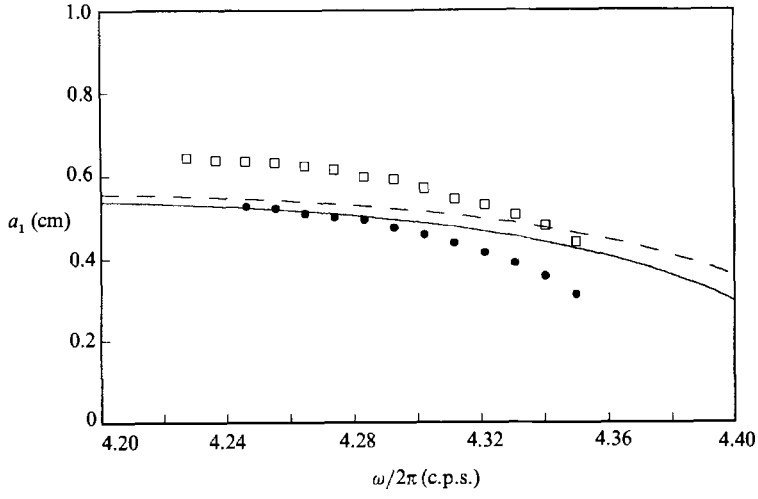

FIGURE 7. Experiments III and IV: wave amplitudes for the (0, 1) mode in the rectangular cylinder. III: calculations (– – –) and measurements (□) with $a_0 = 0.470$ mm. IV: calculations (—) and measurements (●) with $a_0 = 0.425$ mm.

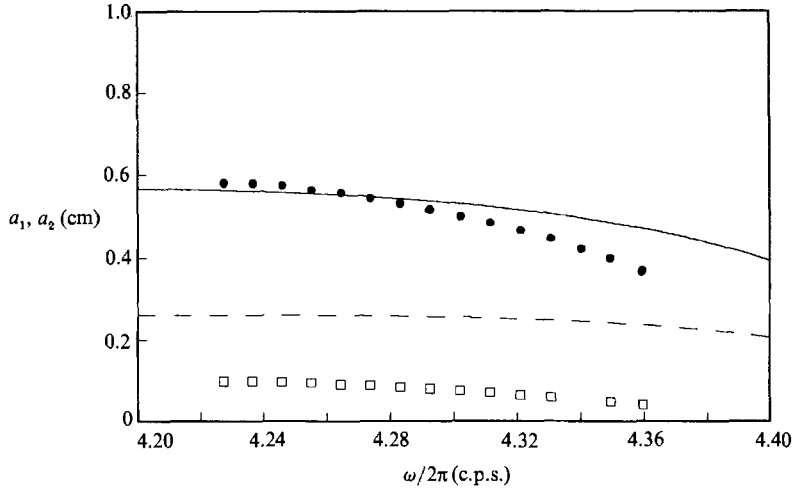

FIGURE 8. Experiment I: amplitudes of the subharmonic a_1 and synchronous a_2 components of the (0, 1) wave in the rectangular cylinder with $a_0 = 0.500$ mm; calculated, (—) and measured (●) subharmonic amplitudes; calculated (– – –) and measured (□) synchronous amplitudes.

than observed in set II. Notice that the measured amplitudes do increase with forcing amplitude, as predicted.

Figure 8 shows the results of set I in figure 5. These experiments were conducted to test how well (2.11) predicts the amplitude of the synchronous component of the wavefield. Unlike the Faraday-wave amplitudes, the synchronous-mode amplitudes are much lower than predicted. Surprisingly, the amplitudes of the Faraday waves in this set of experiments decreased from those in III and IV, although the forcing amplitude and the predicted wave amplitudes increased. In contrast, the amplitudes of the synchronous modes increased from the values in III and IV. The subharmonic waves in I may have been sufficiently nonlinear to have lost more energy to their

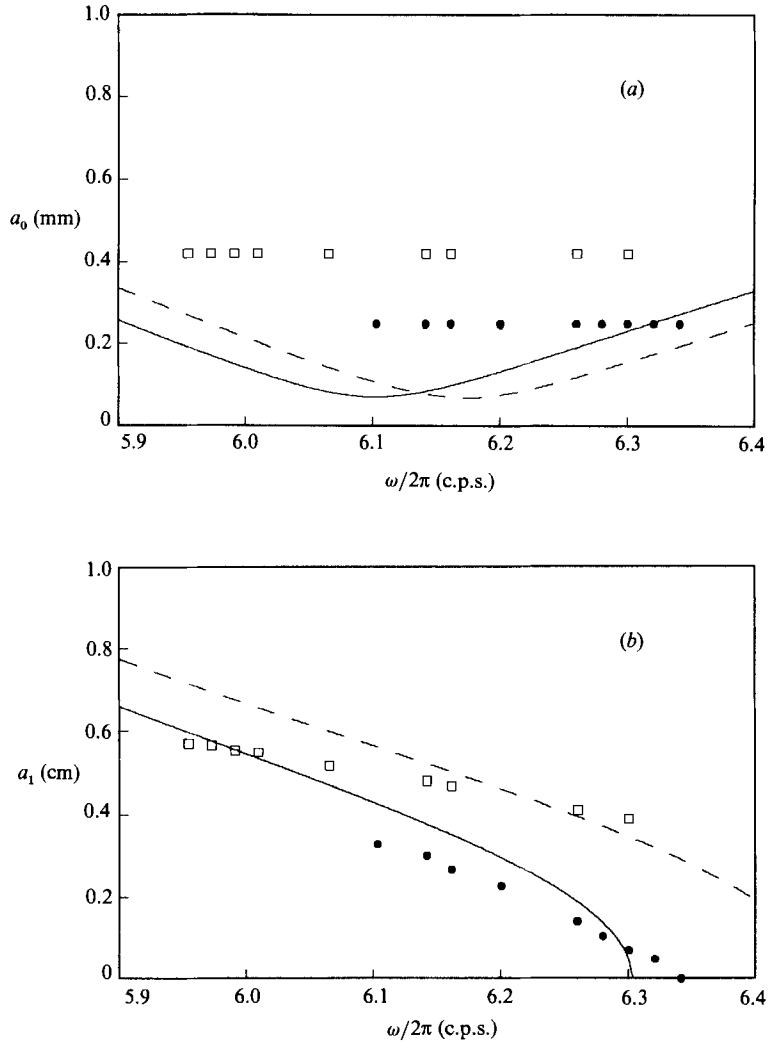

FIGURE 9. Experiments on the (4, 0) mode in the rectangular cylinder with $h = 2.04$ cm and $\delta = 0.026$. (*a*) Stability boundaries: —, $k_{40} = 1.42$ cm^{-1} and $\delta = 0.010$; – – –, $k_{31} = 1.45$ cm^{-1} and $\delta = 0.010$. Location of experiments with: □, $a_0 = 0.419$ mm; ●, $a_0 = 0.248$ mm. (*b*) Wave amplitudes: calculations (– – –) and measurements (□) with $a_0 = 0.419$ mm; calculations (—) and measurements (●) with $a_0 = 0.248$ mm.

superharmonics than predicted by the weakly nonlinear theory (although, $\epsilon = 0.037$ for I). An alternative explanation may be that the experiments of set I are approaching the stability boundary of the (1,1) mode; in consequence of which the single-mode theory may be inapplicable.

Calculations from (2.7)–(2.10) predict amplitudes reasonably well for waves in the circular cylinder. However, they provide only qualitative predictions of amplitudes for waves in the rectangular cylinder. The larger discrepancies in the rectangular cylinder may have occurred because wave damping in the rectangular cylinder is larger than in the circular cylinder and not as adequately predicted by (2.19) (see §4.1). For example, damping due to corner effects may be present, in addition to that from Stokes boundary layers. (See also the last paragraph in §1).

The results of the final set of experiments are shown in figure 9. They consist of measured and predicted amplitudes for wavefields in which only one mode, (4, 0), is observed, but two modes, (4, 0) and (3, 1), are theoretically available for excitation. The experiments are located in the stability space shown in figure 9(*a*). We observed the (4, 0) mode in all of the experiments shown, despite the availability of the (3, 1) mode. Wavefields with frequencies outside the range of those shown were a superposition of the (4, 0) and (3, 1) modes. Since the (4, 0) mode has a smaller measured damping rate ($\delta = 0.026$) than the (3, 1) mode ($\delta = 0.028$), its selection is consistent with the conclusions of §4.1. Nevertheless, (2.5) predicts the excitation of the (3, 1) mode; hence, it appears that the calculation for neutral stability, which takes into account only one mode, is no longer applicable when two modes are available.

Figure 9(*b*) shows the corresponding wave amplitudes. Predictions and measurements are in qualitative agreement, so that the single-mode theory appears to be applicable in this situation. We have expected it to apply here because only one mode was observed and the spatial correlation coefficients (2.16*a*) for the interaction of the (4, 0) and (3, 1) modes are zero.

We thank Janet Becker and Joe Hammack for many helpful comments. This work was supported in part by the Physical Oceanography, Applied Mathematics and Fluid Dynamics/Hydraulics programs of the National Science Foundation, NSF Grant OCE-85-18763, by the Office of Naval Research, Contract N00014-84-K-0137, 4322318 (430), by the DARPA Univ. Res. Int. under Appl. and Comp. Math Program Contract N00014-K-0758 administered by the Office of Naval Research. D.M.H. also gratefully acknowledges the support of an ARCS Fellowship.

REFERENCES

BENJAMIN, T. B. & URSELL, F. 1954 The stability of the plane free surface of a liquid in vertical periodic motion. *Proc. R. Soc. Lond.* A **225**, 505–515.

BLOOMFIELD, P. 1976 *Fourier Analysis of Time Series: An Introduction.* Wiley.

CILIBERTO, S. & GOLLUB, J. P. 1985 Chaotic mode competition in parametrically forced surface waves. *J. Fluid Mech.* **158**, 381–398.

DODGE, F. T., KANA, D. D. & ABRAMSON, H. N. 1965 Liquid surface oscillations in longitudinally excited rigid cylindrical containers. *AIAA J.* **3**, 685–695.

FARADAY, M. 1831 On a peculiar class of acoustical figures; and on certain forms assumed by groups of particles upon vibrating elastic surfaces. *Phil. Trans. R. Soc. Lond.* **121**, 299–340.

GU, X. M., SETHNA, P. R. & NARAIN, A. 1988 On three-dimensional nonlinear subharmonic resonant surface waves in a fluid: Part I – Theory. *J. Appl. Mech.* **55**, 213–219.

KITCHENER, J. A. & COOPER, C. F. 1959 Current concepts in the theory of foaming. *Q. Rev. Chem. Soc.* **13**, 71–97.

MILES, J. W. 1967 Surface-wave damping in closed basins. *Proc. R. Soc. Lond.* A **297**, 459–475.

MILES, J. W. 1984 Nonlinear Faraday resonance. *J. Fluid Mech.* **146**, 285–302.

MILES, J. & HENDERSON, D. 1990 Parametrically forced surface waves. *Ann. Rev. Fluid Mech.* (in press).

SCOTT, J. C. 1979 The preparation of clean water surfaces for fluid mechanics. In *Surface Contamination: Genesis, Detection and Control,* vol. 1 (ed. K. L. Mittal), pp. 477–497. Plenum.

VIRNIG, J. C., BERMAN, A. S. & SETHNA, P. R. 1988 On three-dimensional nonlinear subharmonic resonant surface waves in a fluid: Part II – experiment. *Trans. ASME* E: *J. Appl. Mech.* **55**, 220–224.